## VI. Conclusion

A buoyant, inkjet-printed, paper-based 3-D Lagrangian sensor for real-time flood monitoring has been presented. A new antenna design has been introduced comprising a dipole uniquely oriented on all the faces of a cube to achieve a near isotropic radiation pattern. The antenna performance has been demonstrated in an unconventional lossy medium of water and the sensor is able to communicate across a decent range both while in air as well as while half immersed in water. This work demonstrates a hybrid system utilizing a silicon chip integrated with an inkjet-printed circuit and antenna. This is a step forward in realizing all inkjet-printed, paper-based 3-D electronics.

## References


[1] L. Li, Y. Hong, J. Wang, R. Adler, F. Policelli, S. Habib, D. Irwin, T. Korme, and L. Okello, "Evaluation of the real-time TRMM-based multi-satellite precipitation analysis for an operational flood prediction system in Nzoia Basin, Lake Victoria, Africa," *Nat. Haz.*, vol. 50, pp. 109–123, 2009.

[2] E. Basha, S. Ravela, and D. Rus, "Model-based monitoring for early warning flood detection," in *Proc. 6th ACM Conf. Embedded Network Sensor Syst.*, 2008, pp. 295–308.

[3] M.-C. Effen, D. H. Quintela, R. Jordan, W. Westhoff, and W. Moreno, "Wireless sensor networks for flash-flood alerting," presented at the IEEE Int. Conf. Dev. Cir. Syst., 2004.

[4] N.-B. Chang and D.-H. Guo, "Urban flash flood monitoring, mapping and forecasting via a tailored sensor network system," in *Proc. IEEE Int. Conf. Networking, Sensing Control*, 2006, pp. 757–761.

[5] C. Oroza, A. Tinka, P. K. Wright, and A. M. Bayen, "Design of a network of robotic Lagrangian sensors for shallow water environments with case studies for multiple applications," *Proc. Inst. Mech. Engrg., Part C: J. Mech. Engrg. Sci.*, 2013 [Online]. Available: http://pic.sagepub.com/content/early/2013/02/22/0954406213475947

[6] H. Andersson, A. Manuilskiy, T. U. C. Lidenmark, S. Forsberg, and H.-E. Nilsson, "Inkjet printed silver nanoparticle humidity sensor with memory effect on paper," *IEEE J. Sensors*, vol. 12, no. 6, pp. 1901–1905, Jun. 2012.

[7] R. Vyas, V. Lakafosis, H. Lee, G. Shaker, L. Yang, G. Orecchini, A. Traille, M. M. Tentzeris, and L. Roselli, "Inkjet printed, self powered, wireless sensors for environmental, gas, and authentication-based sensing," *IEEE J. Sensors*, vol. 11, no. 12, pp. 3139–3152, 2011.

[8] B. S. Cook and A. Shamim, "Inkjet printing of novel wideband and high gain antennas on low-cost paper substrate," *IEEE Trans. Antennas Propag.*, vol. 60, no. 9, pp. 4148–4156, 2012.

[9] M. F. Farooqui, R. M. Bilal, H. M. Cheema, and A. Shamim, "A paper based inkjet printed real time location tracking TAG," in *Proc. IEEE MTT-S Int. Microwave Symp. (IMS)*, 2013, pp. 1–4.

[10] J. R. Cooper and M. M. Tentzeris, "Novel "smart cube" wireless sensors with embedded processing/communication/power core for "smart skins" applications," *IEEE Sensors*, pp. 1–4, 2012.

[11] D. Tausch, W. Sattler, K. Wehrfritz, G. Wehrfritz, and H.-J. Wagner, "Experiments on the penetration power of various bullets into skin and muscle tissue," *Int. J. Legal Med.*, vol. 81, no. 4, pp. 309–328, 1978.

[12] A. J. Steckl, "Circuits on cellulose," *IEEE Spectrum*, vol. 50, no. 2, pp. 48–61, 2013.

[13] G. Marrocco, "Gain-optimized self-resonant meander line antennas for RFID applications," *IEEE Antennas Wireless Propag. Lett.*, vol. 2, no. 1, pp. 302–305, Jan. 2003.

[14] Super Glue Gel Dynatex, part no. 49433.

[15] *A True System-on-Chip Solution for 2.4 GHz IEEE 802.15.4 and ZigBee Applications*, [Online]. Available: http://www.ti.com/lit/ds/symlink/cc2530.pdf


# Theory of ESPAR Design With Their Implementation in Large Arrays

Mohammad Ranjbar Nikkhah, Pedram Loghmannia, J. Rashed-Mohassel, and Ahmed A. Kishk

***Abstract*—A generalized formulation as well as a simple design approach is presented for electronically steerable parasitic array radiators (ESPAR). Based on the presented design procedure, a low-cost rectangular dielectric resonator parasitic phased array antenna is designed. An E-plane linear dielectric resonator phased array coupled to symmetric narrow slot apertures is investigated. The driven element is mutually coupled to the parasitic elements and reactive loads are utilized to control the phase to achieve a particular beam scanning direction. The use of low-cost reactive loads instead of expensive conventional phase shifters allows for more economic fabrication. Based on this design, a five elements planar array is designed and measured. In addition, a large array using ESPAR subarrays is presented.**

***Index Terms*—Aperture coupled, dielectric resonator antenna, parasitic elements, phased array.**

## I. Introduction

Phase shifters and true time delays (i.e., Rotman lens) are utilized as crucial beam scanning mechanisms in phased array antenna beam formers. Phase shifters deteriorate the performance of large phased array because of their high losses, particularly above X-band. It is well known that in many cases, the cost of phase shifters may mount up nearly half of the cost of an entire electronically scanned phased array. Therefore, there is a need to develop low cost phased arrays using different approaches.

The Electronically-Steerable Parasitic Array Radiator (ESPAR) antenna is a viable alternative to true time delay for scanning [1]. The basic concept is investigated in [2]. Mutual coupling is used as a mean to excite parasitic elements [3].

ESPAR antennas are considered as attractive adaptive arrays due to their compact size, low cost, and the limited requirements on signal processing. ESPAR antennas are expected to play an important role in future wireless communications. The ESPAR has been presented for small arrays [4].

Unlike reflectarrays, which are excited by a source far from the array elements, the ESPAR antenna is excited by one of the elements in the array while other elements are fed parasitically via electromagnetic mutual coupling. The phase shift between dielectric resonator antennas (DRA) is achieved by varying the reactance of the reactive loadings on

Manuscript received June 21, 2013; revised February 03, 2014; accepted March 02, 2014. Date of publication March 05, 2014; date of current version May 29, 2014.

M. Ranjbar Nikkhah was with the Center of Excellence on Applied Electromagnetic Systems, School of Electrical and Computer Engineering, University of Tehran, Tehran, Iran. He is now with the Poly-Grames Research Center, Ecole Polytechnique (University of Montreal), Montreal, QC H3T 1J4, Canada (e-mail: ranjbar.nikkhah@alumni.ut.ac.ir).

P. Loghmannia is with the Faculty of Electrical Engineering, K. N. Toosi University of Technology, Tehran, Iran.

J. Rashed-Mohassel is with the Center of Excellence on Applied Electromagnetic Systems, School of Electrical and Computer Engineering, University of Tehran, Tehran, Iran.

A. A. Kishk is with the Department of Electrical and Computer Engineering, Concordia University, Montreal, QC H3G 1M8, Canada (e-mail: kishk@encs.concordia.ca).

Color versions of one or more of the figures in this communication are available online at http://ieeexplore.ieee.org.

Digital Object Identifier 10.1109/TAP.2014.2309958

the parasitic DRs. ESPAR arrays suffer from limited scan range around the boresight and high sidelobe level. However, conical radiation patterns and full azimuthal scanning is achieved with low sidelobe level in [5]. For some special cases wideband ESPAR is achieved [6]. A comparative study between the conventional uniform 3-element microstrip antenna array and ESPAR array is investigated [7], [8]. Recently, three elements microstrip H-plane ESPAR antenna with continuous scanning range of $\pm 15^{\circ}$ off the boresight has been reported [9]. The impedance bandwidth of the microstrip ESPAR is narrow and matching of the antenna is difficult to preserve during beam scanning [10]. Unlike patch antennas, DRAs can achieve higher radiation efficiency due to the absence of conduction losses and wider bandwidth [11]. Recently, a new three H-plane DRA-ESPAR mounted on a dielectric substrate and directly excited by microstrip lines has been reported [12].

In this communication, the ESPAR theory is generalized and a simple approach is proposed to obtain the ESPAR design parameters by comparing ESPAR array with a conventional array. Then, an E-plane ESPAR, as well as, the planar case are introduced. In addition, a new concept is proposed to enlarge the array size by using a small ESPAR array as a subarray for a larger array. In [13], the H-plane DRA-ESPAR linear array excited by narrow slots is presented. However, in this article the generalized formulation based on the S-parameters for N elements that require solving N-1 equations is presented. The expansion inspired us to try larger ESPAR array, which have never been tried before. We present a direct relation between conventional array and ESPAR array through which we can design the ESPAR array for certain specifications. Such trial indicated that dielectric resonators ESPAR array is difficult to design for large array as the mutual coupling magnitude decays rapidly for the far away elements making it difficult to achieve the required gain. However, other antenna types may have stronger coupling and smaller mutual coupling decay than DRA. Here, to overcome this problem for the DRA, more than one element has to be directly excited to enhance the coupling to a level that improves the power distribution of the array. Therefore, a large array is designed based on the subarray concept. In order to reduce the grating lobe, an interleaved type of arrangement of the array is used. The ESPAR subarray that is found to be suitable for this configuration is the five element cross-arrangement. However, this has complicated the feeding network design as will be seen later.

## II. ESPAR Design Based on the Comparison With Conventional Array

Our goal is to generalize the design theory of the ESPAR array and simplify the method of determining the required load terminations. This can be done by a simple comparison between the ESPAR and the conventional array of a similar layout. Fig. 1 shows an $\mathrm{N}+1$-element ESPAR. The center element is directly excited. The parasitic elements are loaded with reactive loads having reactances of $\mathrm{x}_1, \mathrm{x}_2, \ldots, \mathrm{x}_\mathrm{N}$. Here, the theory is generalized and presented in terms of the S-parameters of the array. In addition, a simple way to predict the required loadings for a prespecified scanning direction is presented with the help of the analysis of a corresponding conventional array for the first time.

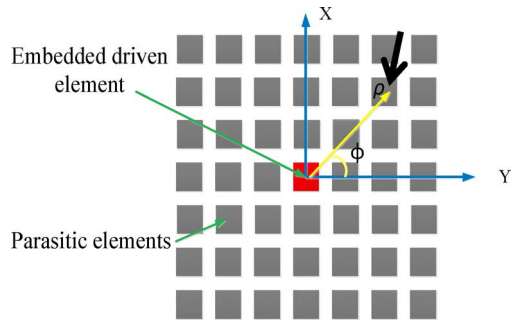


Fig. 1. Schematic diagram of ESPAR phased array.

The N+1-element ESPAR can be assumed as N+1-port network and parasitic elements are loaded with reactive loads. As the element type, array layout, and the antenna ports are determined, the system is described at the center frequency as $[b] = [S][a]$, where $[b]$ and $[a]$ are the backward and incident waves vectors to the antenna ports, respectively, and $[S]$ is the s-matrix that contain all effects of the mutual coupling. Ranking the array elements from 0 to N, Port 0 is the only excited port (driven element). Reactive loads that are represented by their reflection coefficients ($a_i = \Gamma_{\mathrm{L}i} b_i$, for $i \neq 0$ and $i = 1 \ldots N$) terminate the rest of the ports. The reflection coefficients are given as

$$\Gamma_{Li} = \frac{Z_{Li} - Z_{ci}^{*}}{Z_{Li} + Z_{ci}} \quad \text{where } i = 1, 2, 3 \ldots, N \tag{1}$$

where $Z_{Li}$ and $Z_{ci}$ are the termination load impedance and the port impedance of port $i$, respectively. With simple substitutions we can get (2), shown at the bottom of the page.

As the number of elements increases, the array factor can be a good approximation and the pattern multiplication can be acceptable. The array factor can be obtained as,

$$AF(\theta, \phi) = \sum_{i=0}^{N} a_i / a_0 e^{jk_o \rho_i \sin\theta \cos(\phi - \phi_i)} \tag{3}$$

where $\rho_i$ and $\phi_i$ are the radial and azimuthal positions of the $i$'th element in the plane x-y. It should be stated that the array factor in (3) includes the mutual coupling between the elements. Now, (3) can be compared with the array factor of a conventional array of similar layout. In the conventional array, all elements are excited with effective terminal voltages $V_i$ that are normalized to $V_0 = 1$ and contain all the mutual couplings. This desired conventional array factor may be written in the form,

$$AF(\theta, \phi) = \sum_{i=0}^{N} V_i e^{jk_o \rho_i \{\sin\theta \cos(\phi - \phi_i) - \sin\theta_0 \cos(\phi_0 - \phi_i)\}} \tag{4}$$

where $(\theta_0, \varphi_0)$ is the desired scanning direction. Comparing (3) and (4), yields

$$a_i / a_0 = V_i e^{-jk_o \rho_i \sin\theta_0 \cos(\phi_0 - \phi_i)} = V_i e^{-j\psi_i}. \tag{5}$$

$$\begin{pmatrix} \frac{a_1}{a_0} \\ \frac{a_2}{a_0} \\ \bullet \\ \frac{a_n}{a_0} \\ \bullet \\ \frac{a_N}{a_0} \end{pmatrix} = \begin{bmatrix} s_{11} - \frac{1}{\Gamma_1} & s_{12} & \cdots & s_{1n} & \cdots & s_{1N} \\ s_{21} & s_{22} - \frac{1}{\Gamma_2} & \cdots & s_{2n} & \cdots & s_{2N} \\ \bullet & \bullet & \cdots & \bullet & \cdots & \bullet \\ s_{n1} & s_{n2} & \cdots & s_{nn} - \frac{1}{\Gamma_n} & \cdots & s_{\mathrm{n}N} \\ \bullet & \bullet & \cdots & \bullet & \cdots & \bullet \\ s_{N1} & s_{N2} & \cdots & s_{Ni} & \cdots & s_{NN} - \frac{1}{\Gamma_N} \end{bmatrix}^{-1} \begin{pmatrix} -s_{10} \\ -s_{20} \\ \bullet \\ -s_{n0} \\ \bullet \\ -s_{N0} \end{pmatrix}. \tag{2}$$

By substituting (2) into (5), the comparison between the two array factors yields (6) and (7), shown at the bottom of the page. Solving (7) provides all $\Gamma_i$'s. According to (1), $Z_{Li}$ (termination reactive loads) can be obtained. Using these systematic procedures, any linear or planar ESPAR antenna can be designed. For a specific ESPAR topology and S-parameters matrix, (7) may be used in order to determine the required reactive loads. It should be stated that the above procedure is valid for similar or dissimilar elements in the array. However, if the array elements are dissimilar, the radiation patterns of each element might be different. Therefore, the total radiation patterns can be obtained by multiplying each element radiation pattern with its corresponding series element in the array factor summation. The above procedure is used to design a planar DRA-ESPAR of similar elements consisting of a driven element and parasitic dielectric resonator elements.

## III. E-Plane and Planar ESPAR-DRA Considerations

### A. E-Plane ESPAR-DRA

In [12] an H-plane three- element ESPAR array was presented. Here, an E-plane three-element ESPAR array is presented. The main DR (driven element) is fed by a narrow slot. The slot is coupled to a 50 Ω microstrip line, etched on the bottom side of the substrate. The rectangular DRA with a high dielectric constant, $\varepsilon_d = 35.9$, and dimensions, $a = b = 18$ mm, and $h = 8.9$ mm, is placed symmetrically over the narrow slot. The slot is etched on a 62 mil Rogers RT 5870 with $\varepsilon_r = 2.33$ and $\tan\delta = 0.0012$. Two DRAs identical to the driven element are parasitically coupled to the driven DR through the electromagnetic mutual coupling. The phase shift between the DR elements is provided by loading the terminals of the parasitic elements with the proper reactance obtained from the above procedure.

In [12] we presented the performance of the H-plane three-element DRA-ESPAR. It should be noted that the coupling in the E-plane is different from the coupling in the H-plane. The H-plane coupling does not change the polarity of the DRA modes. However, when the elements are much closer to each other with a distance less than a half wavelength, the E-plane polarities of the edge elements modes are opposite to the driven element. Therefore, the values of the reactive loads in the H-plane are of different values. The array in Fig. 2 is analyzed using the full-wave analysis based on the microwave studio (CST). Fig. 3 illustrates the full-wave simulated E-plane and H-plane patterns of the E-plane DRA-ESPAR. The simulated peak gain and scan angles for different loadings are shown in Table I. In addition, the simulated reflection coefficients of the proposed antenna are shown in Fig. 4. It is

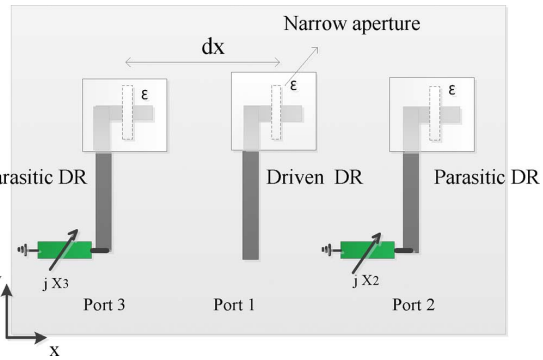


Fig. 2. E-plane ESPAR-DRA (dx = 30 mm).

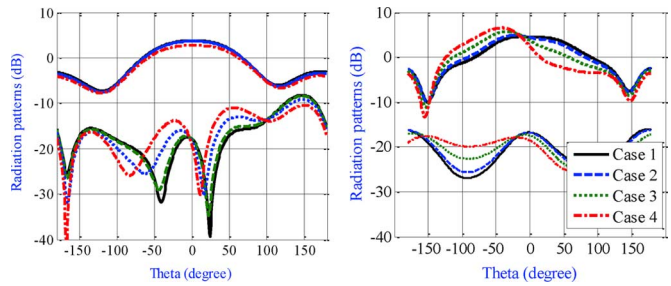


Fig. 3. E-plane (left) and H-plane (right) simulated co- and cross-polarized radiation patterns of the E-plane ESPAR-DRA for different reactive loadings using CST at 2.83 GHz.

interesting to point out that, the impedance matching is maintained at all beam steering angles. It can be noticed that the gain for the E-plane case is lower than the gain of the H-plane array in [12]. The distance between the elements in the E-plane is larger than that in the H-plane.

It should be noticed that the gain increases as the scan angle increases. This is due to the elements' radiation pattern peaks, which are off the boresight direction. One can justify this by considering the three elements as a Yagi-Uda structure having the scanning beam to lean more towards the direction of the beam peak.

In the E-plane ESPAR-DRA, when the middle element is excited and the other two elements are parasitic, the parasitic elements become out of phase from the center element. That explains the reason of the gain reduction. Also, that might be the reason why E-plane ESPAR has never been reported before. E-plane array cannot be avoided whenever

$$[S]\begin{pmatrix} V_1e^{-j\psi_1} \\ V_2e^{-j\psi_2} \\ \bullet \\ V_ne^{-j\psi_n} \\ \bullet \\ V_Ne^{-j\psi_N} \end{pmatrix} - diag\left(\frac{1}{\Gamma_i}\right)\begin{pmatrix} V_1e^{-j\psi_1} \\ V_2e^{-j\psi_2} \\ \bullet \\ V_ne^{-j\psi_n} \\ \bullet \\ V_Ne^{-j\psi_N} \end{pmatrix} = \begin{pmatrix} -s_{1m} \\ -s_{2m} \\ \bullet \\ -s_{nm} \\ \bullet \\ -s_{Nm} \end{pmatrix} \tag{6}$$

$$\begin{pmatrix} \frac{1}{\Gamma_1} \\ \frac{1}{\Gamma_2} \\ \bullet \\ \frac{1}{\Gamma_n} \\ \bullet \\ \frac{1}{\Gamma_N} \end{pmatrix} = \begin{pmatrix} \frac{s_{1m}}{V_1e^{-j\psi_1}} \\ \frac{s_{2m}}{V_2e^{-j\psi_2}} \\ \bullet \\ \frac{s_{nm}}{V_ne^{-j\psi_n}} \\ \bullet \\ \frac{s_{Nm}}{V_Ne^{-j\psi_N}} \end{pmatrix} + \begin{bmatrix} \frac{s_{11}}{V_1e^{-j\psi_1}} & \frac{s_{12}}{V_1e^{-j\psi_1}} & \cdots & \frac{s_{1n}}{V_1e^{-j\psi_1}} & \cdots & \frac{s_{1N}}{V_1e^{-j\psi_1}} \\ \frac{s_{21}}{V_2e^{-j\psi_2}} & \frac{s_{22}}{V_2e^{-j\psi_2}} & \cdots & \frac{s_{2n}}{V_2e^{-j\psi_2}} & \cdots & \frac{s_{2N}}{V_2e^{-j\psi_2}} \\ \bullet & \bullet & \cdots & \bullet & \cdots & \bullet \\ \frac{s_{n1}}{V_ne^{-j\psi_n}} & \frac{s_{n2}}{V_ne^{-j\psi_n}} & \cdots & \frac{s_{nn}}{V_ne^{-j\psi_n}} & \cdots & \frac{s_{nN}}{V_ne^{-j\psi_n}} \\ \bullet & \bullet & \cdots & \bullet & \cdots & \bullet \\ \frac{s_{N1}}{V_Ne^{-j\psi_N}} & \frac{s_{N2}}{V_Ne^{-j\psi_N}} & \cdots & \frac{s_{Ni}}{V_Ne^{-j\psi_N}} & \cdots & \frac{s_{NN}}{V_Ne^{-j\psi_N}} \end{bmatrix}\begin{pmatrix} V_1e^{-j\psi_1} \\ V_2e^{-j\psi_2} \\ \bullet \\ V_ne^{-j\psi_n} \\ \bullet \\ V_Ne^{-j\psi_N} \end{pmatrix} \tag{7}$$

TABLE I
DIFFERENT LOADINGS IN E-PLANE DRA-ESPAR (d = 30 mm)

| Case | L-2 | L-3 | Peak gain (dB) | $\theta_0$ (deg.) (achieved) | $\theta_0$ (deg.) (desired) |
|---|---|---|---|---|---|
| 1 | 0.591 pF | 0. 569 pF | 4.6 | 0 | 0 |
| 2 | 0.515 pF | 0.653 pF | 4.8 | 23 | 22 |
| 3 | 0.330 pF | 0.968 pF | 5.7 | 34 | 35 |
| 4 | 0.149 pF | 1.61 pF | 6.5 | 42 | 40 |

L-2, L3 ARE FOR LOAD 2 AND LOAD 3.

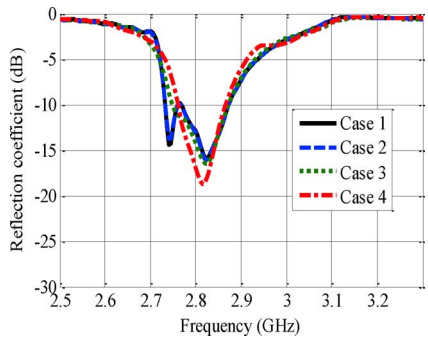


Fig. 4. Simulated reflection coefficients of the E-plane ESPAR-DRA for different reactive loadings using CST.

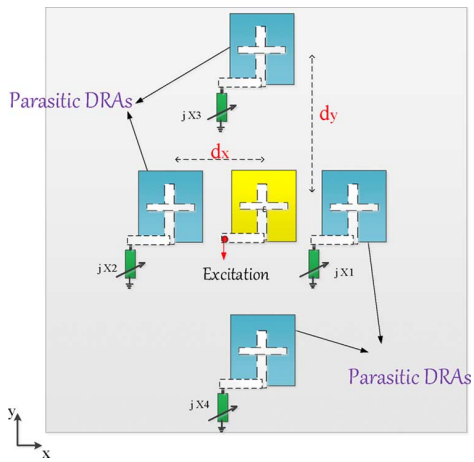


Fig. 5. Planar ESPAR- DRA with 5 elements ($d_x = 22$ and $d_y = 30$ mm).

a planar array is designed. In order to reduce such an effect, the coupling between the elements in the E-plane has to be reduced, which is possible by increasing the separation between the elements.

### B. Planar ESPAR-DRA

ESPAR-DRA phased array in a planar configuration is investigated. The array in Fig. 5 is analyzed using full-wave analysis based on CST. It is interesting to point out that, the impedance matching is relatively maintained at all beam steering angles according to Fig. 6. In a conventional array, all elements are active. Mutual coupling affects the matching of the elements significantly. As the main beam scans, effective induced voltages between the antenna element terminals change that is in turn change the terminal elements current and consequently change the effective input impedance. It should be mentioned that manufacturing errors might have occurred with case 3 of Fig. 6. In addition, according to [14], the immediate dielectric constant materials that have sandwiched the slot will affect the slot length. The slot length is inversely proportional to the effective dielectric constant of the surrounding materials (in our work, $\varepsilon_r$ is high). Hence, the proper length

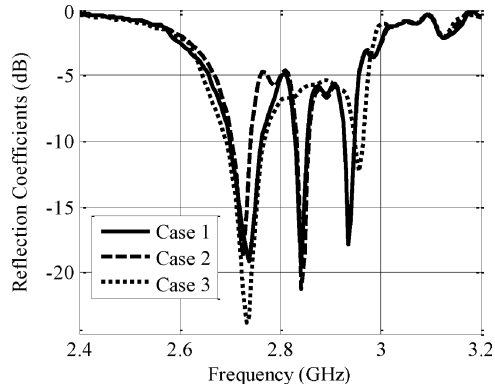


Fig. 6. Measured reflection coefficients of the planar DRA-ESPAR.

TABLE II
SIMULATED RESULTS FOR DIFFERENT LOADINGS OF PLANAR ESPAR-DRA

| Case | L-1 | L- 2 | L-3 | L- 4 | G (dB) | $(\theta_0, \varphi_0)^o$ (achieved) | $(\theta_0, \varphi_0)^o$ (desired) |
|---|---|---|---|---|---|---|---|
| 1 | 56.5 nH | 6.22 pF | 0.563 pF | 0.289 pF | 6.4 | (36,59) | (35,60) |
| 2 | 1.49 nH | 2.92 pF | 0.389 pF | 0.406 pF | 5.18 | (33, 1) | (35, 0) |
| 3 | 158 pF | 1170 pF | 1.04 pF | 0.118 pF | 7.61 | (43,89) | (45, 90) |

L-1, L-2, L-3, AND L-4 ARE FOR LOAD 1, 2, 3, AND 4.

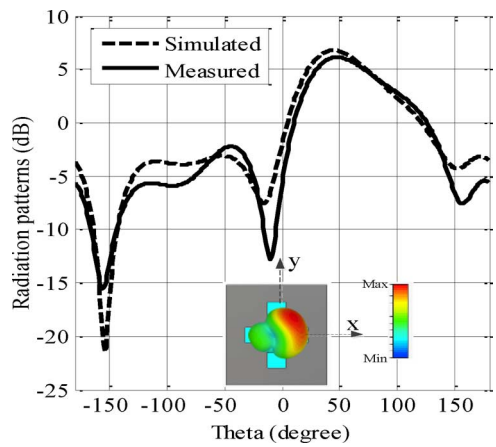


Fig. 7. Measured and simulated results for case 1 at 2.83 GHz ($\phi_0 = 60$ deg.).

for the slot can be used and therefore impedance matching will be improved as the slot length changes from 14.4 mm to 12 mm. Thus, the reflection coefficients have been improved.

Here as a proof of concept, reactive loads are used to load the DR radiators. In practice and for real time performance, simple and low-cost varactors and their bias networks can be used to change the reactive elements from a positive to a negative value [15], [16]. Furthermore, [15] illustrates a simple voltage controlled varactor that is combined with an open stub to generate both positive and negative reactances. The simulated peak gain and scan angle for different loadings are shown in Table II. Measured and simulated radiation patterns for different scanning azimuthal planes, $\phi_0 = 60°$, 0°, and 90° and the maximum possible elevation angles are shown in Figs. 7, 8, and 9, respectively. The antenna is built as shown in Fig. 10. The reactive loadings are inserted between the microstrip lines and the ground plane.

Compared to the DRAs excited directly by microstrip lines presented in [12], the main advantages (in view of antenna characteristics) of the DRA arrays excited by a slot are as follow: First, the main advantage

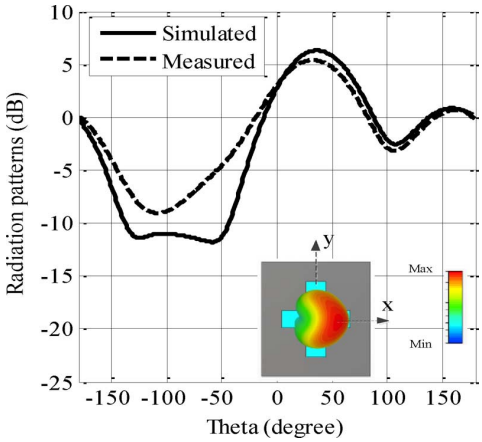


Fig. 8. Measured and simulated results for case 2 at 2.83 GHz ($\phi_0 = 0$ deg.).

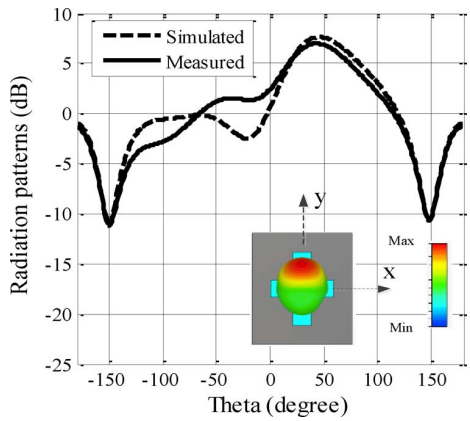


Fig. 9. Measured and simulated results for case 3 at 2.83 GHz ($\phi_0 = 90$ deg.).

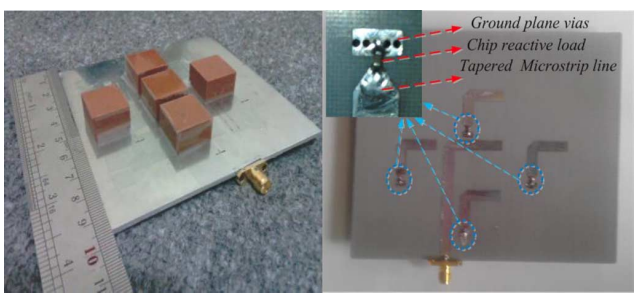


Fig. 10. Photo of front (left) and back (right) of the five-element array.

is elimination of the radiation effects of microstrip circuits in the upper half space. Second, all biasing circuits and loads are moved to the back of the array. Third, the DR is now sitting on the ground plane and not on the dielectric substrate and therefore eliminating the possible presence of surface waves that might contribute to the upper half space radiation. However, the disadvantage is the radiation of the slots to the back lower half space. This can be reduced or eliminated by using a reflector in the back of the slots. The bandwidth of the present antennas is relatively narrower due to the high permittivity of the dielectric (35.9) and there is a trade-off between the size and the bandwidth. The radiation bandwidth for the array (Fig. 10) is 5% and the radiation patterns are stable for this radiation bandwidth.

## IV. Large Array Concept

The small crossed planar ESPAR array is incorporated as a subarray in a larger planar array. Due to the ability of scanning of the ESPAR

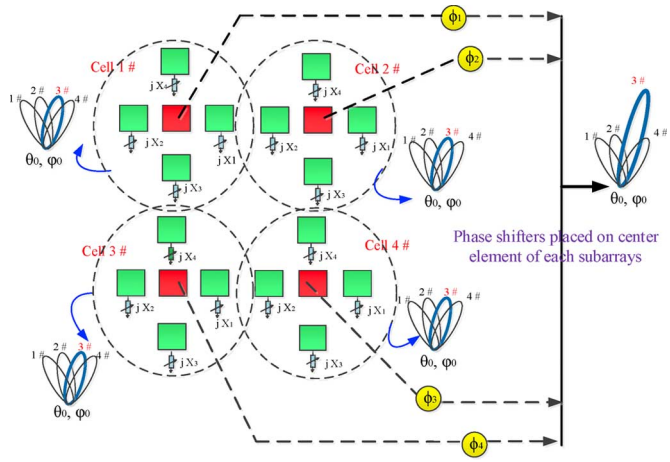


Fig. 11. Sketch for the concept of large planar array of ESPAR-DRA.

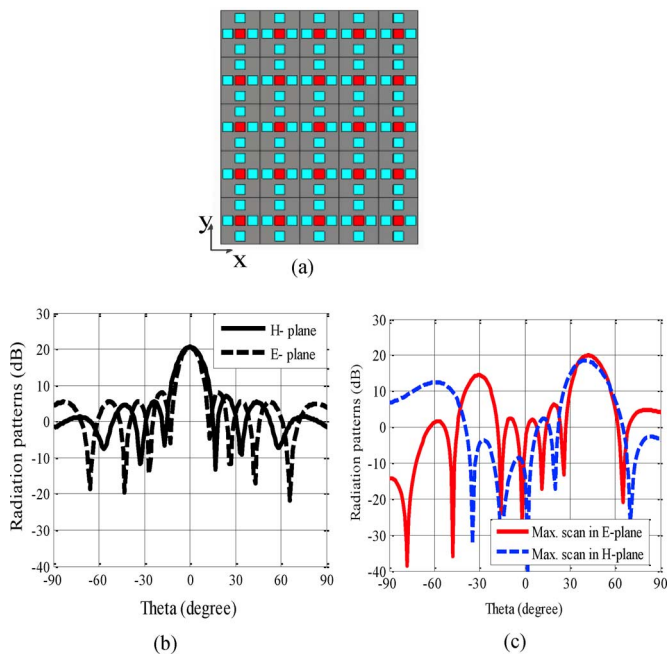


Fig. 12. Simulated radiation patterns at f = 2.83 GHz for different scanning direction, (a) $5 \times 5$ conventional regular rectangular array, (b) boresight, (c) scan in E-plane ($\phi_0 = 90°$) and H-plane ($\phi_0 = 0°$).

array without phase shifters, it is used as a single element (subarray) of a larger array without any concern for large sidelobes or inordinate gain loss while scanning. As such higher scan range and high directivity will be attained, while the pattern will exhibit a much smaller half-power beamwidth. This way, we can have a larger array with few excited elements embedded within the planar array. The concept is like using more than one excited element in the array as to strengthen the power level of the parasitic elements far away from the driven element.

If the subarray is used in the scanning array, it is required to have the subarray with a pattern beam directed towards the intended scanning direction. Then the driven elements should be provided with the required phasing to direct the beam of the large array to the same direction as the subarray. The relative phase with the reactive loads will be the same with respect to the driven element. Therefore, the driven elements are those that require the phase shifters. It is interesting to point out that the sidelobe level of the large array can also be controlled by changing the power distributions of the driven elements through the feeding network. This concept is shown in Fig. 11.

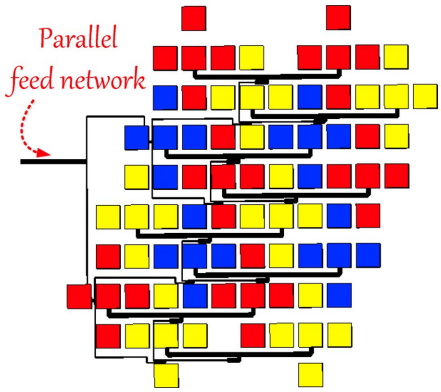


Fig. 13. Large planar ESPAR-DRA in interleaved arrangement.

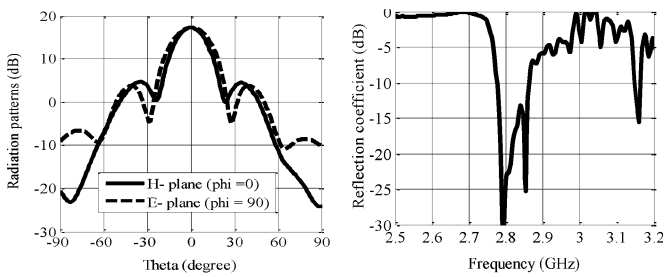


Fig. 14. Full-wave simulation for the array in Fig. 14. (a) Radiation patterns at 2.83 GHz, and (b) the simulated $S_{11}$.

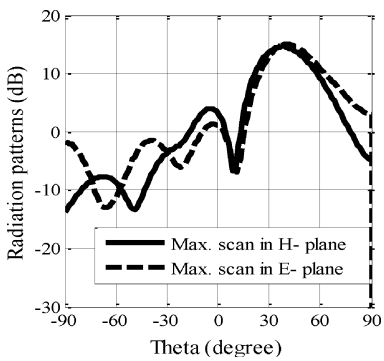


Fig. 15. Full-wave simulation radiation patterns for maximum scanning in E plane and H-plane at 2.83 GHz for the array in Fig. 14 (with no feeding network).

If the five-element crossed subarrays placed in a conventional regular rectangular array of $5 \times 5$ elements, the radiation patterns for a boresight radiation is shown in Fig. 12, providing a gain of about 21 dB with aperture efficiency of more than 90%. Fig. 12 also shows the radiation patterns of two other scanning directions, scanning in $\phi_0 = 90^\circ$, and scanning in $\phi_0 = 0^\circ$. The radiation patterns are showing the presence of the grating lobes. The grating lobe in the $\phi_0 = 90^\circ$ is higher than the one in the $\phi_0 = 0^\circ$ as the distance between the subarray in $\phi_0 = 90^\circ$ is larger than the distance in $\phi_0 = 0^\circ$. The grating lobe will be higher in the case of scanning in the diagonal plane.

To eliminate possible grating lobes, interleaved arrangement of subarrays is used as shown in Fig. 13. This arrangement reduces the distance between the subarrays and as such eliminating the grating lobes. Also it allows for the scanning in any azimuthal plane without grating lobes. A complete array has been modeled in CST as shown in Fig. 13 as the array is fed by conventional parallel feed network. Fig. 14(a) and (b) show the radiation patterns and reflection coefficient for boresight mode, respectively. The maximum scan in the elevation direction, $\theta^\circ$, in $\phi_0 = 90^\circ$ and $\phi_0 = 0^\circ$ are shown in Fig. 15. As can be seen the grating lobes are eliminated in this configuration. However, the feeding network required more complicated layout.

## V. Conclusion

A novel inexpensive parasitic phased array antenna using DRAs has been introduced. The array factor computation for these antennas has been presented and utilized. A general formulation, relating the ESPAR array to the conventional array has been presented. This formulation has easily predicted the proper loading of the antenna terminals for a specified beam scanning direction. Arrays have been matched for all the scanning directions. The large array has been designed with ESPAR subarrays. An interleaved arrangement has been implemented to eliminate or reduce the grating lobes.

## References

[1] R. Schlub and D. V. Thiel, "Switched parasitic antenna on a finite ground plane with conductive sleeve," *IEEE Trans. Antennas Propag.*, vol. 52, no. 5, pp. 1343–1347, May 2004.

[2] R. F. Harrington, "Reactively controlled directive arrays," *IEEE Trans. Antennas Propag.*, vol. AP-26, no. 3, May 1978.

[3] M. R. Nikkhah, J. Rashed-Mohassel, and A. A. Kishk, "High-gain aperture coupled rectangular dielectric resonator antenna array using parasitic elements," *IEEE Trans. Antennas Propag.*, vol. 61, no. 4, pp. 2318–2321, Apr. 2013.

[4] H. Kawakami and T. Ohira, "Electrically steerable passive array radiator (ESPAR) antennas," *IEEE Antennas Propag. Mag.*, vol. 47, no. 2, pp. 43–50, Apr. 2005.

[5] W. Chen, J. Sun, X. Wang, and Z. Feng, "Design of planar ESPAR antenna by using sidelobe reduction algorithm," presented at the Int. Conf. on Microwave and Millimeter Wave Technology, 2007.

[6] A. Sutinjo, M. Okoniewski, and R. H. Johnston, "An octave band switched parasitic beam-steering array," *IEEE Antennas Wireless Propag. Lett.*, vol. 6, pp. 211–214, 2007.

[7] J. J. Luther, S. Ebadi, and X. Gong, "A comparison of microstrip patch ESPAR array and uniformly-illuminated array performance," presented at the IEEE Antennas and Propagation Society Int. Symp. (APSURSI), July. 2012.

[8] Y. Yusuf and X. Gong, "A low-cost patch antenna phased array with analog beam steering using mutual coupling and reactive loading," *Antennas Wireless Propag. Lett.*, vol. 7, pp. 81–84, 2008.

[9] J. J. Luther, S. Ebadi, and X. Gong, "A microstrip patch electronically steerable parasitic array radiator (ESPAR) antenna with reactance-tuned coupling and maintained resonance," *IEEE Trans. Antennas Propag.*, vol. 60, no. 4, pp. 1803–1813, Apr. 2012.

[10] Y. Yusuf and X. Gong, "Beam-steerable patch antenna array using parasitic coupling and reactive loading," presented at the IEEE AP-S Int. Symp., Honolulu, Hi, USA, 2007.

[11] K. M. Luk and K. W. Leung, *Dielectric Resonator Antenna*. Baldock, U.K.: Research Studies Press, 2003.

[12] M. R. Nikkhah, J. Rashed-Mohassel, and A. A. Kishk, "Compact low-cost phased array of dielectric resonator antenna using parasitic elements and capacitor loading," *IEEE Trans. Antennas Propag.*, vol. 61, no. 4, pp. 2318–2321, Apr. 2013.

[13] M. R. Nikkhah, J. Rashed-Mohassel, and A. A. Kishk, "ESPAR_DRA phased array," presented at the IEEE In. Conf. on Wireless and Information Technology, 2012.

[14] A. A. Kishk, "Experimental study of broadband embedded dielectric resonator antennas excited by a narrow slot," *IEEE Antenna Wireless Propag. Lett.*, vol. 4, pp. 79–81, 2005.

[15] T. D. Dimousios, S. A. Mitilineos, S. C. Panagiotou, and C. N. Capsalis, "Design of a corner-reflector reactively controlled antenna for maximum directivity and multiple beam forming at 2.4 GHz," *IEEE Trans. Antennas Propag.*, vol. 59, no. 4, pp. 1132–1139, Apr. 2011.

[16] C. Sun, N. C. Karmakar, and T. Ohira, "Experimental studies of radiation pattern of electronically steerable passive array radiator smart antenna," presented at the IEEE Antennas and Propagation Society Int. Symp., 2003.